

Benefits of Using Non-consolidated Domain Influence in Meshless Local Petrov-galerkin (Mlpg) Method for Solving Lefm Problems

Hashim N. Al-Mahmud, Haider K. Mehbes, Ameen A. Nassar*

Mechanical Engineering Department, College of Engineering, University of Basrah

*Corresponding Author: ameenaledani@yahoo.com

Copyright © 2014 Horizon Research Publishing All rights reserved.

Abstract This paper presents an efficient meshless method in the formulation of the weak form of local Petrov-Galerkin method MLPG. The formulation is carried out by using an elliptic domain rather than conventional isotropic domain of influence. Therefore, the method involves an MLPG formulation in conjunction with an anisotropic weight function. In the elliptic weight function, each node has three characteristic indicated that were major radius, inner radius, and the direction of the local domain. Furthermore, the space that will be covered by the elliptical domain will be less than the area of the circle (isotropic) at the same main diameter. This means leaving many points of integration are not necessary. Therefore, the computational cost will be decreased. MLPG method with the elliptical domain is used in solving problems of linear elastic fracture mechanism LEFM. MATLAB and Fortran codes are used for obtaining the results of this research. The results were compared with those presented in the literature which shows a reduction in the computational cost up to 15%, and an error criteria enhancement up to 25%.

Keywords Meshless Methods, Local Petrov-Galerkin Method MLPG, Elliptic Domain

1. Introduction

Meshless (MFree) methods, as alternative numerical approaches to eliminate the well-known drawbacks in the finite element and boundary element methods have attracted much attention in the past decade, due to their flexibility, and due to their potential in neglecting the need for the human-labor intensive process of constructing geometric meshes in a domain. There are a number of MFree methods has been developed named according to the technique used in the formulation of the method the major differences in these meshless methods come from the interpolation techniques used [1-4].

In recent decades Mfree methods in computational mechanics have a great attention in solving practical engineering problems in heat transfer, fluid mechanics, and applied mechanics [5-7], especially those problems with discontinuities or moving boundaries. The numerical solution by the traditional finite element method (FEM) of fracture mechanics problems with arbitrary dynamic cracks is limited to simple cases. This is because solution of growing discontinuities requires time consuming remeshing at every time step. For this reason adaptive FEM has become essential. However adaptive remeshing and mapping of variables is a difficult, computationally expensive task and is a source of cumulative numerical errors. The development of meshless methods has enabled the solution of growing cracks without remeshing. Nevertheless, these methods continue to be computationally expensive because of the large nodal densities in meshless methods for an accurate solution. Therefore there is a constant effort to improve the accuracy without increasing the degrees of freedom The main objective of MFree methods is to get rid of or at least alleviate the difficulty of meshing the entire structure ,by only adding or deleting nodes in the entire structure.

A truly meshless method shadow elements are inevitable as in Element-Free Galerkin Methods [8-9] called Meshless Local Petrov-Galerkin Method (MLPG) have been successfully developed in [10-16] for solving linear and non-linear boundary problems [17]. The MLPG method uses local weak forms over a local sub-domain and shape functions from the moving least-squares (MLS) approximation [18]. In the MLS approximation, each node in the global domain Ω has two sub-domains the 1st is the domain of influence Ω_x , in which a trial function of compact support is used as a weight function. The weight function determines the intensity of the effect of a node at various points in its domain of influence, the 2nd is a sub-domain for the test function Ω_s (Integral Domain) which often similar in shape but smaller than the trial function. These nodal trial and test functions are centered with maximum value at the nodes (which are the centers of the domains Ω_x and Ω_s),

respectively, and, in general, vanish at the boundaries $\partial\Omega_x$ and $\partial\Omega_s$ of Ω_x and Ω_s , respectively having a bell/tent shape. The local domains Ω_x and Ω_s can be of arbitrary shapes, such as circle, and square rectangle (conventional domains) in 2D geometries as shown in Figures (1-a,b and c), and spheres, square or rectangular parallelepipeds in 3D geometries [19-20]. The sizes of Ω_x and Ω_s can be arbitrary, different from each other, and different for each node, in general. Essential boundary conditions are enforced while using the meshless approximations, approximately by using a penalty formulation and Lagrange multipliers [1].

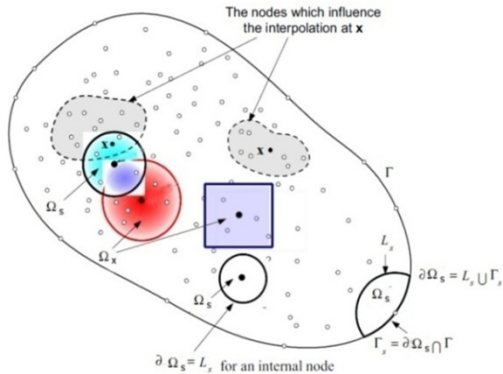


Figure (1-a). Schematics of the MLPG method [1]

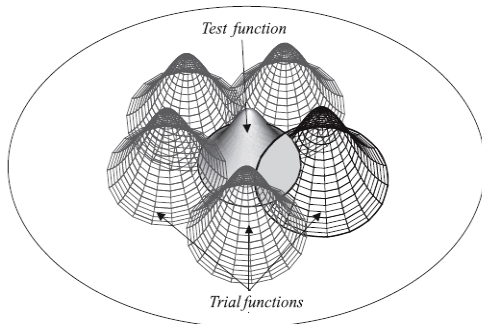


Figure (1-b). Schematics of the trial and test functions in Ω [5].

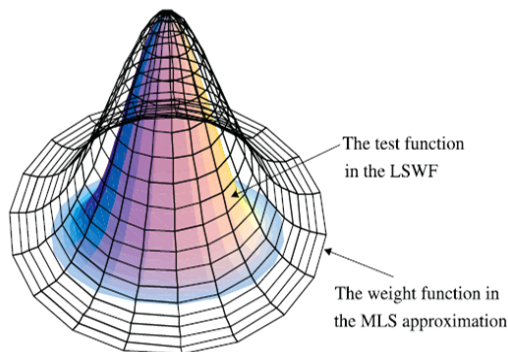


Figure (1-c). The test function in the Local Symmetric Weak Form (LSWF) and the weight function in the MLS approximation[11]

The nodal influence domain is usually considered having a consolidated form in the shape of a circle or sphere. In the

$$P^T(x, y) = (1, x, y, \sqrt{r} \cos(\theta/2), \sqrt{r} \sin(\theta/2), \sqrt{r} \sin(\theta/2) \sin \theta, \sqrt{r} \cos(\theta/2) \sin \theta), m=7 \quad (7)$$

MLPG, accuracy and effectiveness are dependent on the nodal domain of influence and type of the weight function. In this work, non-consolidated (anisotropic) weight function in the elliptic form is introduced to improve the efficiency of the MLPG with an anisotropic support in some problems. In the using non-consolidated weight functions, the influence domain of each node may vary with direction. As a consequence, the definition of the influence domain based on non-consolidated weight function, improves the numerical efficiency of MLPG. In such case, the influence domain of each node can be determined so that the nodal overlapping decreases. Thus, good results can be achieved with less computational efforts.

2. MLS Approximation

It has been shown that moving least-square methods and weight functions share many features for the constructing the approximation of the solution. In the MLS technique that presented by [18], the approximation $u^h(X)$ is expressed as the inner product of a vector of the polynomial basis $P(X)$ and a vector of the coefficient $a(X)$.

$$u^h(X) = P^T(X)a(X) = \sum_{i=1}^m P_i(X)a_i(X) \quad (1)$$

where m denotes the number of terms in the basis. In two dimensions a complete polynomial basis of order m is given by

$$P^T(x, y) = (1, x, y, x^2, xy, y^2, \dots, x^m, \dots, x^m y^{m-k}, \dots, y^m) \quad (2)$$

For bi-linear, the basis function is considered as

$$P^T(x, y) = (1, x, y, xy), m=4 \quad (3)$$

Also, the linear basis is provided by

$$P^T(x, y) = (1, x, y), m=3 \quad (4)$$

Vector of unknown parameters that depends on x is given as

$$a(X) = (a_1(x), a_2(x), \dots, a_m(x)) \quad (5)$$

These basis functions are not required to be polynomials as shown in equations (3) and (4). For problems involving cracks, a convenient way of capturing $1/\sqrt{r}$ stress-singularity in linear-elastic fracture mechanics is calculated by using [2]

$$P^T(x, y) = (1, x, y, \sqrt{r}), m=4 \quad (6)$$

or

Where r and θ are polar coordinates with the crack tip as the origin. Equations (6) and (7) represent fully enriched and partially enriched basis functions, respectively.

In equation (1), the coefficient vector, $a(X)$ is determined by minimizing a weighted discrete L_2 norm, defined as

$$J(X) = \sum_{I=1}^n w(X - X_I) [P^T(X_I) a(X) - u_I]^2 \quad (8)$$

Where n is the number of nodes I such that $w(x - x_I) > 0$; $w_I(x) = w(x - x_I)$ is the weight function associated with node I which is non-zero over a limited support called the influence domain of node I .

Equation (8) can also be written as [1]

$$J(X) = [P.a(X) - u]^T W [P.a(X) - u] \quad (9)$$

Where

$$u^T = \{u_1, u_2, \dots, u_n\} \quad (10)$$

$$P = [P_{ij}]_{n \times m} = \begin{bmatrix} 1 & x_1 & y_1 & x_1 y_1 \\ 1 & x_2 & y_2 & x_2 y_2 \\ \vdots & \vdots & \vdots & \vdots \\ 1 & x_n & y_n & x_n y_n \end{bmatrix} \quad (11)$$

$$W(X) = (w_{ij})_{n \times n} = \begin{bmatrix} w(X - X_1) & 0 & \dots & 0 \\ 0 & w(X - X_2) & \dots & 0 \\ \vdots & \vdots & \ddots & \vdots \\ 0 & 0 & \dots & w(X - X_n) \end{bmatrix} \quad (12)$$

The stationarity of $J(X)$ with respect to $a(X)$ yields

$$\frac{\partial J}{\partial a} = A(X)a(X) - B(X)u = 0 \quad (13)$$

Hence

$$a(X) = A^{-1}(X)B(X)u \quad (14)$$

$$A(X) = P^T W(X) P \quad (15)$$

$$= w(X - X_I) \begin{bmatrix} 1 & x_1 & y_1 & x_1 y_1 \\ x_1 & x_1^2 & x_1 y_1 & x_1^2 y_1 \\ y_1 & y_1 x_1 & y_1^2 & x_1 y_1^2 \\ x_1 y_1 & x_1^2 y_1 & x_1 y_1^2 & x_1^2 y_1^2 \end{bmatrix} + \dots +$$

$$w(X - X_n) \begin{bmatrix} 1 & x_n & y_n & x_n y_n \\ x_n & x_n^2 & x_n y_n & x_n^2 y_n \\ y_n & y_n x_n & y_n^2 & x_n y_n^2 \\ x_n y_n & x_n^2 y_n & x_n y_n^2 & x_n^2 y_n^2 \end{bmatrix}$$

$$B(X) = P^T W(X) \quad (16)$$

$$= [w(X - X_1)P(X_1) \quad w(X - X_2)P(X_2) \quad \dots \quad w(X - X_n)P(X_n)]$$

The MLS approximants can be defined as

$$u^h(X) = \sum_{I=1}^n \varphi_I(X) u_I = \Phi(X) u \quad (17)$$

Where the shape function $\Phi_I(X)$ is

$$\Phi_I(X) = P^T(X) A^{-1}(X) B_I(X) \quad (18)$$

The partial derivatives of $\Phi_I(X)$ can be obtained as follows

$$\Phi_{I,i}(X) = \sum_{j=1}^m \left\{ p_{j,i} (A^{-1} B)_{jI} + p_j (A_i^{-1} B + A^{-1} B_{,i})_{jI} \right\} \quad (19)$$

Where

$$A_i^{-1} = -A^{-1} A_i A^{-1} \quad (20)$$

In which $(\)_{,i} = \frac{\partial(\)}{\partial x_i}$.

3. The MLPG Weak Formulation

Consider the following two-dimensional elasto-statics problem on the domain Ω bounded by the boundary Γ [1,10]:

$$\sigma_{ij,j} + b_i = 0, \text{ in } \Omega, \quad (21)$$

where σ_{ij} is the stress tensor, b_i is the body force, a repeated index implies summation over the range of the index, the rectangular Cartesian coordinates and employing the boundary conditions gives;

$$u_i = \bar{u}_i \text{ on } \Gamma_u \quad (22)$$

$$t_i \equiv \sigma_{ij} n_j = \bar{t}_i \text{ on } \Gamma_t \quad (23)$$

where \bar{u}_i and \bar{t}_i are the prescribed displacements and tractions, respectively, on the boundary Γ_u and the boundary Γ_t , and n_j is the unit outward normal to the boundary Γ . Γ_u and Γ_t are complementary subsets of Γ .

A generalized local weak form of eq. (21) and Eqs. (22),(23) over a local sub-domain Ω_s can be written as follows [1]:

$$\int_{\Omega_s} (\sigma_{ij,j} + b_i) v_i d\Omega - \int_{\Gamma_{su}} \alpha (u_i - \bar{u}_i) v_i d\Gamma = 0 \quad (24)$$

where u_i and v_i are the trial and the test functions, respectively, and Γ_{su} is the part of the boundary $\partial\Omega_s$ over which essential boundary conditions are specified. In general, $\partial\Omega_s = \Gamma_s \cup L_s$ with Γ_s being the part of the local boundary located on the global boundary and L_s being the other part of local boundary over which no boundary condition is specified, i.e., $\Gamma_s = \partial\Omega_s \cap \Gamma$ and $\Gamma_s = \partial\Omega_s \setminus L_s$ see Figure (1-a). In eq. (24) α is a penalty parameter ($\alpha \gg \text{Young's}$

modulus/Length) which is used to impose the essential boundary conditions. Also, the dimensions of α are such that the two terms in eq. (24) have the same units. α could be a function of \mathbf{x} but is usually taken to be a constant.

Using $\sigma_{ij,j} v_i = (\sigma_{ij} v_i)_{,j} - \sigma_{ij} v_{i,j}$ and the divergence theorem in eq. (24) leads to

$$\int_{\partial\Omega_S} \sigma_{ij} n_j v_i d\Gamma - \int_{\Omega_S} (\sigma_{ij} v_{i,j} - b_i v_i) d\Omega - \alpha \int_{\Gamma_{su}} (u_i - u_i v_i) d\Gamma = 0 \quad (25)$$

Applying the natural boundary condition gives;

$$\int_{L_S} t_i v_i d\Gamma + \int_{\Gamma_{su}} t_i v_i d\Gamma + \int_{\Gamma_{st}} \bar{t}_i v_i d\Gamma - \int_{\Omega_S} (\sigma_{ij} v_{i,j} - b_i v_i) d\Omega - \alpha \int_{\Gamma_{su}} (u_i - u_i v_i) d\Gamma = 0 \quad (26)$$

In order to simplify equation (26), the test functions v_i are chosen such that they vanish on L_S . This can be accomplished by using the weight function w_i in the MLS approximation as also the test function v_i , but the radius r_i of the support of the weight function is replaced by the radius r_0 of the local domain Ω_S . Using these test functions and rearranging eq. (26) gives the Local Symmetric weak form (LSWF);

$$\begin{aligned} & \int_{\Omega_S} \sigma_{ij} v_{i,j} d\Omega + \alpha \int_{\Gamma_{su}} u_i v_i d\Gamma - \int_{\Gamma_{su}} t_i v_i d\Gamma \\ & = \int_{\Gamma_{st}} \bar{t}_i v_i d\Gamma \\ & + \alpha \int_{\Gamma_{su}} \bar{u}_i v_i d\Gamma + \int_{\Omega_S} b_i v_i d\Omega \end{aligned} \quad (27)$$

For 2-D problems, two independent sets of test functions should be applied in eq. (27) which gives

$$\begin{aligned} & \int_{\Omega_S} \sigma_{ij} v_{ki,j} d\Omega + \alpha \int_{\Gamma_{su}} u_i v_{ki} d\Gamma - \int_{\Gamma_{su}} t_i v_{ki} d\Gamma \\ & = \int_{\Gamma_{st}} \bar{t}_i v_{ki} d\Gamma \\ & + \alpha \int_{\Gamma_{su}} \bar{u}_i v_{ki} d\Gamma + \int_{\Omega_S} b_i v_{ki} d\Omega \end{aligned} \quad (28)$$

where v_{ki} is the i th component of the k th test function. For simplicity, eq. (28) can be written in matrix form as:

$$\int_{\Omega_S} \epsilon_v \sigma d\Omega + \alpha \int_{\Gamma_{su}} \mathbf{v} u d\Gamma - \int_{\Gamma_{su}} \mathbf{v} \mathbf{t} d\Gamma = \int_{\Gamma_{st}} \mathbf{v} \bar{\mathbf{t}} d\Gamma + \alpha \int_{\Gamma_{su}} \mathbf{v} \bar{\mathbf{u}} d\Gamma + \int_{\Omega_S} \mathbf{v} \mathbf{b} d\Omega \quad (29)$$

where ϵ_v denotes the strain matrix derived from the test functions, and σ is the stress vector derived from the trial functions. That is,

$$\sigma = \begin{Bmatrix} \sigma_{11} \\ \sigma_{22} \\ \sigma_{12} \end{Bmatrix} \equiv \begin{Bmatrix} \sigma_{xx} \\ \sigma_{yy} \\ \sigma_{xy} \end{Bmatrix}, \epsilon_v = \begin{bmatrix} \epsilon_{11}^{(1)} & \epsilon_{22}^{(1)} & \gamma_{12}^{(1)} \\ \epsilon_{11}^{(2)} & \epsilon_{22}^{(2)} & \gamma_{12}^{(2)} \end{bmatrix} \equiv \begin{bmatrix} \epsilon_{xx}^{(1)} & \epsilon_{yy}^{(1)} & \gamma_{xy}^{(1)} \\ \epsilon_{xx}^{(2)} & \epsilon_{yy}^{(2)} & \gamma_{xy}^{(2)} \end{bmatrix} \quad (30)$$

where the superscript i denotes the i th test function. Functions \mathbf{v} , \mathbf{u} , \mathbf{t} , and \mathbf{b} are defined as follows:

$$\mathbf{v} = \begin{bmatrix} v_{11} & v_{12} \\ v_{21} & v_{22} \end{bmatrix}, \mathbf{u} = \begin{Bmatrix} u_1 \\ u_2 \end{Bmatrix}, \mathbf{t} = \begin{Bmatrix} t_1 \\ t_2 \end{Bmatrix}, \mathbf{b} = \begin{Bmatrix} b_1 \\ b_2 \end{Bmatrix} \quad (31)$$

The two sets of test functions \mathbf{v} in eq. (31) should be linearly

independent. The simplest choice for \mathbf{v} is

$$v_{ij} = v \delta_{ij} \text{ or } \mathbf{v} = v \mathbf{I},$$

where δ_{ij} is the Kronecker delta and \mathbf{I} is the identity matrix. As long as the union of all local sub-domains covers the global domain, the equilibrium equations (21) and the boundary conditions (22),(23) will be satisfied in the global domain Ω and on its boundary Γ respectively.

4. Discretization of the Weak Form

Substituting the MLS approximation eq. (17) into eq. (29) and summing over all nodes leads to the following discretized system of linear equations:

$$\begin{aligned} & \sum_{j=1}^n \int_{\Omega_S} \epsilon_v(\mathbf{x}, \mathbf{x}_i) \mathbf{D} \mathbf{B}_j u_j d\Omega + \\ & \alpha \sum_{j=1}^n \int_{\Gamma_{su}} \mathbf{v}(\mathbf{x}, \mathbf{x}_i) \mathbf{S} \phi_j u_j d\Gamma - \\ & \sum_{j=1}^n \int_{\Gamma_{su}} \mathbf{v}(\mathbf{x}, \mathbf{x}_i) \mathbf{N} \mathbf{D} \mathbf{S} \mathbf{B}_j u_j d\Gamma = \int_{\Gamma_{st}} \mathbf{v}(\mathbf{x}, \mathbf{x}_i) \bar{\mathbf{t}} d\Gamma + \\ & \alpha \int_{\Gamma_{su}} \mathbf{v}(\mathbf{x}, \mathbf{x}_i) \bar{\mathbf{S}} \mathbf{u} d\Gamma + \int_{\Omega_S} \mathbf{v}(\mathbf{x}, \mathbf{x}_i) \mathbf{b} d\Omega \end{aligned} \quad (32)$$

where $\mathbf{v}(\mathbf{x}, \mathbf{x}_i)$ is the value at \mathbf{x} of the test function, corresponding to node i , and

$$\mathbf{N} = \begin{bmatrix} n_1 & 0 & n_2 \\ 0 & n_2 & n_1 \end{bmatrix} \quad (33)$$

$$\mathbf{B}_j = \begin{bmatrix} \phi_{j,1} & 0 \\ 0 & \phi_{j,2} \\ \phi_{j,2} & \phi_{j,1} \end{bmatrix} \quad (34)$$

$$\mathbf{D} = \bar{E}/(1 - \bar{\nu}^2) \begin{bmatrix} 1 & \bar{\nu} & 0 \\ \bar{\nu} & 1 & 0 \\ 0 & 0 & (1 - \bar{\nu})/2 \end{bmatrix} \quad (35)$$

We note that

$$\bar{E} = \begin{cases} E & \text{for plane stress} \\ E/(1 - \nu^2) & \text{for plane strain} \end{cases}, \bar{\nu} = \begin{cases} \nu & \text{for plane stress} \\ \nu/(1 - \nu) & \text{for plane strain} \end{cases} \quad (36)$$

$$\mathbf{S} = \begin{bmatrix} S_1 & 0 \\ 0 & S_2 \end{bmatrix}, S_i = \begin{cases} 1 & \text{if } u_i \text{ is prescribed on } \Gamma_u, \\ 0 & \text{if } u_i \text{ is not prescribed on } \Gamma_u. \end{cases} \quad (37)$$

Eq. (32) can be simplified into the following system of linear algebraic equations in \mathbf{u}_j

$$\sum_{j=1}^N K_{ij} U_j = f_i \quad i = 1, 2, \dots, N \quad (38)$$

where N is the total number of nodes. The so-called ‘‘stiffness’’ matrix \mathbf{K} and the ‘‘load’’ vector \mathbf{f} are defined by

$$K_{ij} = \int_{\Omega_S} \epsilon_v(\mathbf{x}, \mathbf{x}_i) \mathbf{D} \mathbf{B}_j d\Omega + \alpha \int_{\Gamma_{su}} \mathbf{v}(\mathbf{x}, \mathbf{x}_i) \mathbf{S} \phi_j d\Gamma - \int_{\Gamma_{su}} \mathbf{v}(\mathbf{x}, \mathbf{x}_i) \mathbf{N} \mathbf{D} \mathbf{S} d\Gamma \quad (39)$$

$$f_i = \int_{\Gamma_{st}} \mathbf{v}(\mathbf{x}, \mathbf{x}_i) \bar{\mathbf{t}} d\Gamma + \alpha \int_{\Gamma_{su}} \mathbf{v}(\mathbf{x}, \mathbf{x}_i) \bar{\mathbf{S}} \mathbf{u} d\Gamma + \int_{\Omega_S} \mathbf{v}(\mathbf{x}, \mathbf{x}_i) \mathbf{b} d\Omega \quad (40)$$

5. The Influence of Domain Form

The shape functions θ_i are obtained from the window

functions, these functions have influence domain of the node. The domain size is defined by the so called dilatation parameter or smoothing length. It is critical to solution accuracy, stability and plays the role of the element size in the finite element method. The final characteristics of weight functions are its functional forms. The weight function should be continuous and positive in its support. Some commonly used weight functions are the Gaussian weight function and the quartic spline weight function[10]. They are given, respectively in equation (41) and (42).

$$w_i(\mathbf{x}) = \begin{cases} \frac{\exp[-(d_i/c_i)^{2k}] - \exp[-(r_i/c_i)^{2k}]}{1 - \exp[-(r_i/c_i)^{2k}]} & 0 \leq d_i \leq r_i \\ 0 & d_i \geq r_i \end{cases} \quad (41)$$

$$w_i(\mathbf{x}) = \begin{cases} 1 - 6\left(\frac{d_i}{r_i}\right)^2 + 8\left(\frac{d_i}{r_i}\right)^3 - 3\left(\frac{d_i}{r_i}\right)^4 & 0 \leq d_i \leq r_i \\ 0 & d_i \geq r_i \end{cases} \quad (42)$$

Here $d_i = |\mathbf{x} - \mathbf{x}_i|$ is the distance from the sampling point \mathbf{x} to the node \mathbf{x}_i , and r_i is the radius of the domain of influence for the weight function w_i . The parameters c_i and k in eq.(41) control the shape of the Gaussian weight function w_i . The parameter k can be taken as 1 in eq. (41). So far, there is no theory to determine an optimal value of the parameter c_i and is chosen empirically. It is suggested that c_i defined as the distance from node \mathbf{x}_i to the third nearest neighboring node. The domain of influence r_i can be chosen as $r_i / c_i \geq 3.5$ so that the weight function w_i covers sufficientAlso, it should be small enough to retain the local characteristic of the approximationnumber of nodes to ensure the non-singularity of A in eq.(18) see Figure (2-a).

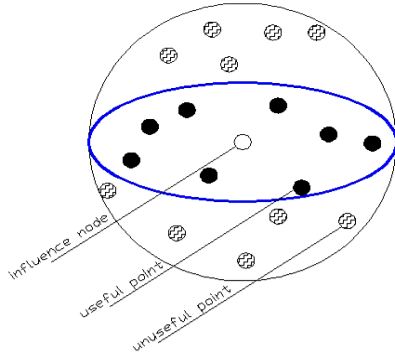


Figure (2-a).

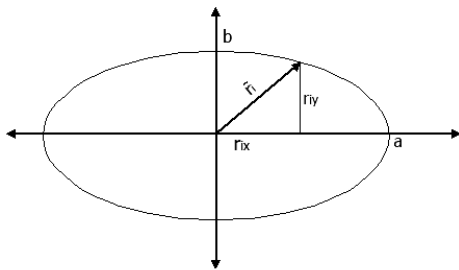


Figure (2-b).

Figure 2. Requirement Representation of Elliptic Domain, and Circular Domain to the Integrations Points

In elliptic weight functions, each node has a major radius of influence a , a minor radius of influence b (where $a = b$ for circular domain) and an angle θ that determines the direction of the maximum radius of the influence ellipse. The influence elliptic domain of a node is determined by three parameters in contrast to one in the circular domain weights. The availability of more controlling parameters for determination of the influence domain of each node helps to increase computational efficiency of MLPG method. The radius of influence of the circular domain r_i is modified to the elliptic form \bar{r}_i

$$\left(\frac{r_{ix}}{a}\right)^2 + \left(\frac{r_{iy}}{b}\right)^2 = 1 \quad (43)$$

Also,, it can be write in general form:

$$\bar{r}_i = \sqrt{r_{ix}^2 + r_{iy}^2} \quad (44)$$

Where r_{ix} , r_{iy} are a normalized horizontal and vertical distance from the sampling point \mathbf{x} to the node \mathbf{x}_i on $\partial\Omega_s$ respectively, see Figure (2-b).

6. The MLPG Solution Algorithm

- MODELING: constructing the problem domain (nodal configuration).
- INPUT: provides the data required for running the solution.
- DMAT: creates the 3×3 constitutive D-matrix.
- GAUS: locates the Gaussian integration points in the natural plane.
- INFLUD: calculates the domain of influence and domain of integration for every node.
- XYQPO: calculates the sub-domain portion of the stiffness K.
- WCOUNT: calculates number of nodes whose weight functions $w(\mathbf{x}_i) > 0$.
- TESTFUN: calculates the value of the test function v_i for the given influence node.
- ABM: calculates the matrix A, the matrix B and their derivatives.
- PVE: calculates the basis vectors and their x, y derivatives.
- SHAPE: calculates the shape function ϕ_i and its x, y derivatives.
- NSTIFF: performs the numerical integration for the stiffness K over the nodal domain.
- BCAPLY: performs the numerical integration of the load vector f.
- BKCAL: performs the numerical integration of the boundary portion of the stiffness matrix K.
- OUTPUT: is for the output of displacements and stresses over the whole domain.

7. Numerical Results

Example 1. This example involves the Timoshenko beam;

consider a beam of dimensions $L \times D$, subjected to a parabolic traction at the free end as shown in Figure (3). The beam is considered to be of unit depth and is in plane stress state. This problem was numerically solved by MLPG with conventional domains previously by [1,21]. The parabolic traction is given by

$$t_y(y) = -\frac{P}{2I} \left(\frac{D^2}{4} - y^2 \right) \quad (45)$$

Where $I = \frac{D^3}{12}$ is the second moment of area. The exact displacement solution and exact stresses for this problem are

$$u_x(x, y) = -\frac{Py}{6EI} \left[(6L-x)x + (2+\nu) \left(y^2 - \frac{D^2}{4} \right) \right] \quad (46)$$

$$u_y(x, y) = \frac{Py}{6EI} \left[3\nu y^2(L-x) + (4+5\nu) \frac{D^2 x}{4} + (3L-x)x^2 \right] \quad (47)$$

$$\sigma_x(x, y) = -\frac{P(L-x)y}{I} \quad (48)$$

$$\sigma_{xy}(x, y) = -\frac{P}{2I} \left(\frac{D^2}{4} - y^2 \right) \quad (49)$$

$$\sigma_y(x, y) = 0 \quad (50)$$

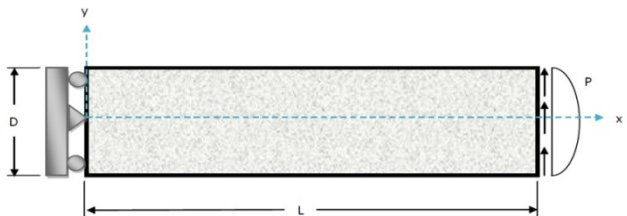


Figure 3. Cantilever beam under an end load.

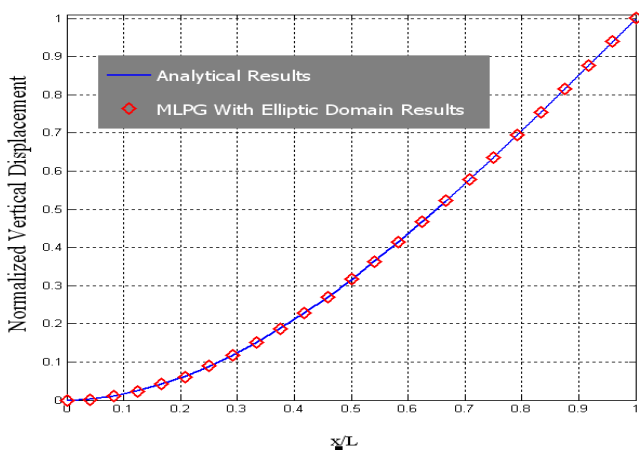


Figure 4. Normalized vertical displacement of a cantilever beam under an end loading

In this paper, the parameters for cantilever beam are material properties as $E = 1$, $\nu = 0.25$ and the beam

dimensions are $D = 4$ and $L = 24$. Shear force is $P = 1$. Regular uniform nodal configurations with number of nodes are 100, 115, and 125. At the circular domain, the problem is solved by using the MLS approximation, with a support size of $(2.3 \times \text{nodal distance})$, and a test size of $(0.6 \times \text{nodal distance})$. While in the anisotropic domain, elliptical nodal support of radius 2.3 times from longer nodal spacing and 1.95 from smaller nodal spacing are employed in x and y direction respectively.

In Table 1, the vertical displacement in the end of beam that is calculated by MLPG is compared with the exact solution at three nodal configurations. By the error criteria, this table shows excellent agreement between MLPG and the analytical solution, particularly in the results of the elliptic domain.

Table 1. Comparison of Error at Vertical Displacement End of Beam

Nodes	Error %	
	Elliptic Domain	Circular Domain
25 x 5	0.25	0.33
23 x 5	2.31	2.64
20 x 5	2.60	2.75

Furthermore, reduction of computational cost is verified. Table 2 clears that the time of computation in the elliptic domain is less than the time of computation in the circle domain. This is due to less value of nodes in Equation (8) when the elliptic domain is used.

Table 2. Comparison of Time Cost of Elliptic and Circle Domain

Nodes	Time of computation (time unit)	
	Elliptic Domain	Circular Domain
25 x 5	3.0292	3.5541
23 x 5	2.882	3.0101
20 x 5	2.3788	2.4343

Example 2. Figure (5-a) displays a rectangular plate with a central crack loaded by an axial tensile traction. Basic parameters are $L=52$ mm, $D=20$ mm, $\bar{t}=0.4H(t)$ Gpa, $E=76$ GPa, poisson's ratio $\nu = 0.286$, $\alpha = 10^7$ MPa/m density $\rho=2450$ Kg/m³ and $a=12$ mm.

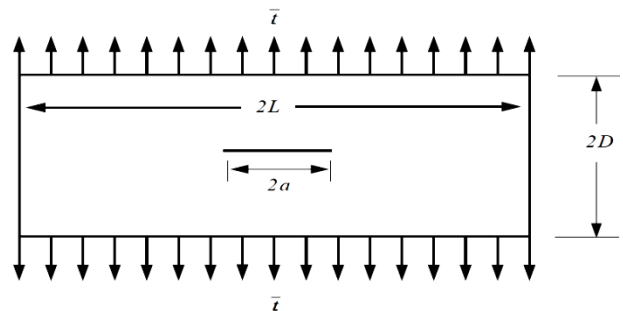


Figure 5-a. A schematic sketch of the centrally cracked plate

A plane strain state of deformation is supposed in computing. Due to the symmetry of the problem about two centroidal axes, only a quadrant of the plate is considered and discretized using 2534 nodes see Figure (5-b) . 9×9 Gauss points are used in a sub-domain Ω_s , 9 Gauss points are used on each section of L_s and Γ_s for numerical integration. The enrichment of nodes at crack tip can be cleared in Figure (5-b). In the MLS approximation, the linear basis function and the Gaussian weight function for both circular and elliptic sub-domains Ω_s are used. The present results, using elliptical sub-domains Ω_s with a major radius of influence $a=r_i$, minor radius of influence $b=0.75r_i$ and an angle $\theta=0$ that determines the direction of the maximum radius of the influence ellipse, are showing in Figures (6, 7, and 8).

These Figures set the variation of stresses σ_x , σ_y and σ_{xy} with the distance to the tip is made at a certain constant time. Results of an anisotropic domain (elliptic domain) have a good agreement compared with the results of reference [22] which is obtained using a circular domains Ω_s , where (a) equals (b) for circular domain , in addition the formulation here is more efficient as it demonstrated in example one. Finally, The ratio of the elapsed time for solving the problem with elliptic domain to circular domain is equal to 0.742.

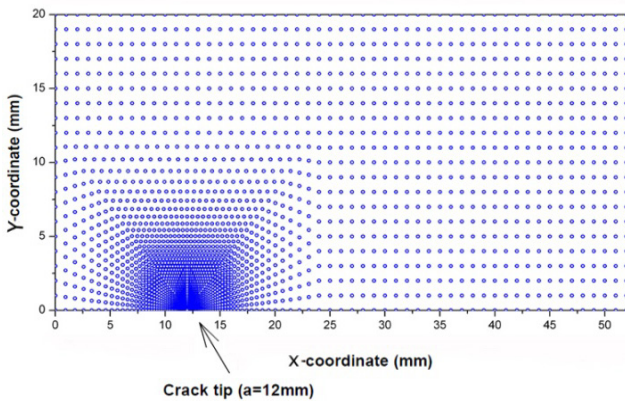


Figure 5-b. The nodal mesh for one quarter of the centrally cracked plate

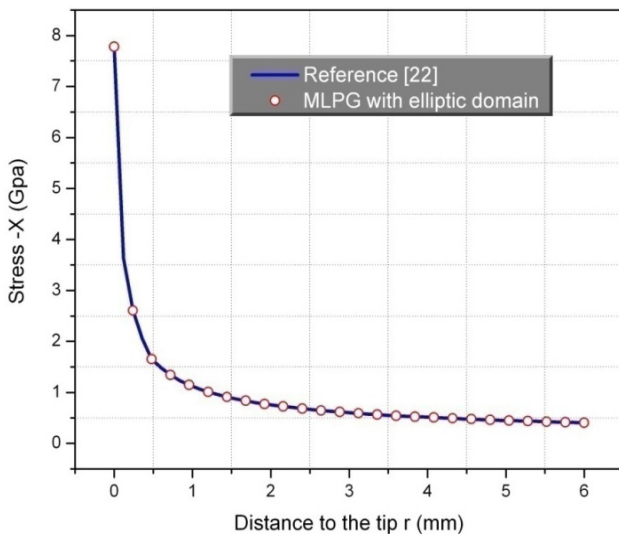


Figure 6. The variation of stress σ_x with the distance to the tip

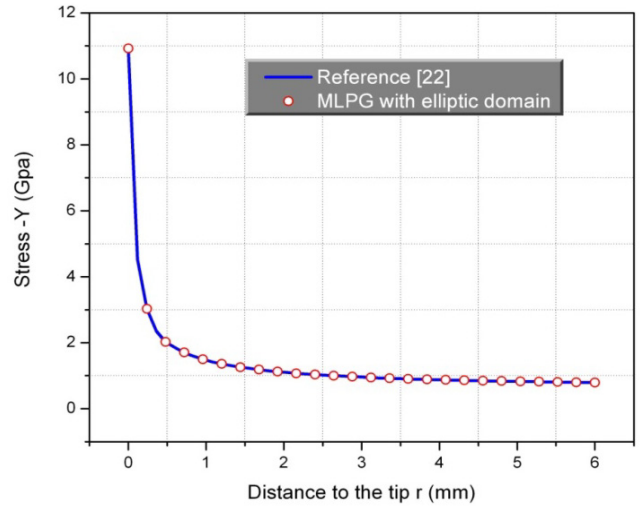


Figure 7. The variation of stress σ_y with the distance to the tip

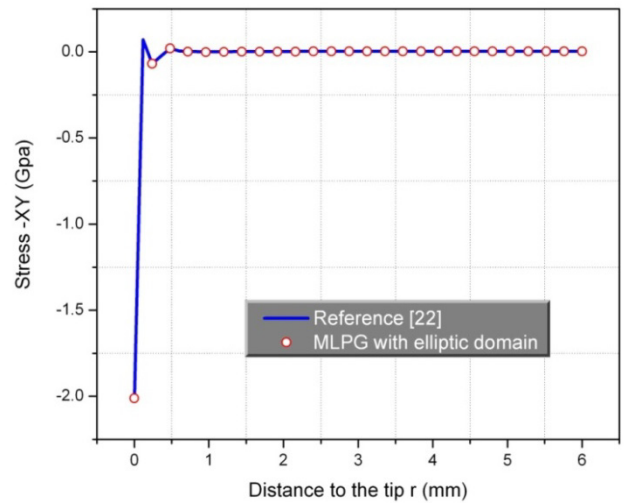


Figure 8. The variation of stress σ_{xy} with the distance to the tip

8. Conclusions

- Elliptic domain of influence is used local weak form method, particularly in the Meshless Local Petro-Galerkin method MLPG, to study the possibility of using this local domain in the computational mechanics.
- This domain changes the behavior of work of the used weight function in extracting the data from the nodes because in the elliptic support each node has three characteristic indications that are major radius, inner radius, and the direction of major local domain.
- The space that is covered by the elliptic domain is less than the area of the circle domain at the same main diameter, and this reduces the computational time of the required calculation. Thus, using this domain, influence domain of a node is determined by three parameters in contrast to one in the other domains.
- The availability of more controlling parameters for

determination of the influence domain of each node helps to increase computational efficiency of MLPG method as it clear in reducing the time cost up to 15% and the results error up to 25%.

- This paper can be extended by changing the direction of major local domain in the calculation or by using in dynamic elasticity problems, as well as in the use of the domain in the other advanced applications.

REFERENCES

- [1] G.R. Liu., "Meshfree methods-moving beyond finite element method", 2nd edition, Book (2010), CRC Press LLC,.
- [2] V. P. Nguyena, T. Rabczuk, S. Bordas, and M. Duflot, "Meshless methods: A review and computer implementation aspects", *Math. and Comp. in Simulation* 79 (2008) 763–813.
- [3] Satya N. Atluri , Shengping Shen "The Meshless Local Petrov-Galerkin (MLPG) Method: A Simple & Less-costly Alternative to the Finite Element and Boundary Element Methods", *CMES*, vol.3, no.1, pp.11-51, 2002.
- [4] S. N. Atluri, J. Sladek, V. Sladek, T. Zhu "The local boundary integral equation (LBIE) and it's meshless implementation for linear elasticity", *Computational Mechanics* 25 (2000) 180-198.
- [5] H. Lin , S.N. Atluri "The Meshless Local Petrov-Galerkin (MLPG) Method for Solving Incompressible Navier-Stokes Equations", *CMES*, vol.2, no.2, pp.117-142, 2001.
- [6] H. Lin, S.N. Atluri "Meshless Local Petrov-Galerkin (MLPG) Method for Convection-Diffusion Problems", *CMES*, vol.1, no.2, pp.45-60, 2000.
- [7] Z. D. Han, H. T. Liu, A. M. Rajendran, S. N. Atluri "The Applications of Meshless Local Petrov-Galerkin (MLPG) Approaches in High-Speed Impact, Penetration and Perforation Problems", *CMES*, vol.14, no.2, pp.119-128, 2006.
- [8] T. Belytschko, Y. Y. Lu, and L. Gu, "Element-Free Galerkin Methods", *International Journal for Numerical Methods in Engineering*, Vol. 37, pp. 229-256, 1994.
- [9] J. Dolbow, and T. Belytschko, "An Introduction to Programming the Meshless Element Free Galerkin Method", *Achieves of Computational Mechanics*, Vol.15, No. 3, pp. 207-241, 1998.
- [10] S. N. Atluri, T. Zhu "New concepts in meshless methods", *Int J Numer Methods Eng.* 47, 537-556(2000).
- [11] S. N. Atluri , T. Zhu " A new Meshless Local Petrov-Galerkin (MLPG) approach in computational mechanics ", *Computational Mechanics* 22 (1998) 117-127
- [12] H.-K. Ching ,R. C. Batra " Determination of Crack Tip Fields in Linear Elastostatics by the Meshless Local Petrov-Galerkin (MLPG) Method ", *CMES*, vol.2, no.2, pp.273-289, 2001.
- [13] Z.Tang, S. Shen , S.N. Atluri " Analysis of Materials with Strain-Gradient Effects: A Meshless Local Petrov-Galerkin(MLPG) Approach, with Nodal Displacements only", *CMES*, vol.4, no.1, pp.177-196, 2003.
- [14] J. Sladek1, V. Sladek1, S.N. Atluri " Meshless Local Petrov-Galerkin Method in Anisotropic Elasticity", *CMES*, vol.6, no.5, pp.477-489, 2004.
- [15] S. N. Atluri, T.-L. Zhu" The meshless local Petrov-Galerkin (MLPG) approach for solving problems in elasto-statics", *Computational Mechanics* 25 (2000) 169-179 © Springer-Verlag 2000.
- [16] Shengping Shen, S. N. Atluri " Multiscale Simulation Based on The Meshless Local Petrov-Galerkin (MLPG) Method", *CMES*, vol.5, no.3, pp.235-255, 2004.
- [17] Z. D. Han, A.M. Rajendran, S.N. Atluri" Meshless Local Petrov-Galerkin (MLPG) Approaches for Solving Nonlinear Problems with Large Deformations and Rotations", *CMES*, vol.10, no.1, pp.1-12, 2005.
- [18] P. Lancaster and K. Salkauskas "Surfaces Generated by Moving Least Squares Methods", *Mathematics of Computation*, Vol. 37, pp. 141-158, 1981.
- [19] Q. Li , S. Shen , Z. D. Han, and S. N. Atluri " Application of Meshless Local Petrov-Galerkin (MLPG) to Problems with Singularities, and Material Discontinuities, in 3-D Elasticity", *CMES*, vol.4, no.5, pp.571-585, 2003.
- [20] Z. D. Han ,S. N. Atluri "Meshless Local Petrov-Galerkin (MLPG) approaches for solving 3D Problems in elasto-statics", *CMES*, vol.6, no.2, pp.169-188, 2004.
- [21] S. N. Atluri, Z. D. Han1 and A.M. Rajendran," A New Implementation of the Meshless Finite Volume Method, Through the MLPG "Mixed" Approach"*CMES: Computer Modeling in Engineering & Sciences*, vol.6, no.6, pp.491-513, 2004
- [22] Liu Kaiyuan , Long Shuyao , Li Guangyao "A simple and less-costly meshless local Petrov-Galerkin (MLPG) method for the dynamic fracture problem", Elsevier Ltd, *Engineering Analysis with Boundary Elements* 30 (2006) 72–76.